Computational fluid dynamic modelling of two phase flow in a hydrocyclone

by M.J. Leeuwner* and J.J. Eksteen†

Paper written on project work carried out in partial fulfillment of MSc Eng (Mineralprocessing. Eng.) degree

Synopsis

Computational fluid dynamic (CFD) modelling is used to research the complex flow structures that exist in a hydrocyclone. By simulation of a two phase (water and air) flow system, the internal flow and multiphase interactions are investigated. The suitability of CFD modelling as a design tool is further evaluated by examining the effect of varying device dimensions. Three hydrocyclone geometries, used in previous studies, are specified. A transient simulation approach, which employs the Reynolds Stress Model as turbulence model and the Volume of Fluid model as multiphase model, is followed. Results are validated qualitatively against experimental measurements from the previous studies.

Keywords: CFD modelling, hydrocyclone, Reynolds stress model, multiphase flow

Nomenclature

Greek symbols

α_q	volume fraction of phase q
δ	Kronecker delta
ε	kinetic dissipation rate
ρ	density
ϕ	pressure strain

Other symbols

C_{ij}	convection term
$D_{ij}{}^L$	molecular diffusion
$D_{ij}{}^T$	turbulent diffusion
F_{ij}	system rotation production
G_{ij}	buoyancy production
m	rate of mass transfer
P_{ij}	stress production
t	time
u,v	velocity magnitude
x	distance

Subscripts

i,j,k	space coordinates
p,q	phases

Introduction

The hydrocyclone is a simple device that is widely applied in the chemical and mineral processing industries for purposes such as liquid clarification, slurry thickening, solids, washing and solids, classification. The reasons for the hydrocyclone's popularity are its simple design and operation, compact structure, high capacity, low running costs and versatility[1].

Separation and classification within the hydrocyclone are brought about by a centrifugal force that develops as swirling flow is induced in its body. In spite of the hydrocyclone's simple construction and operation, this swirling flow behaviour is very complex. The complex features include turbulent flow, high preservation of vorticity, vortex breakdown phenomena and reverse flow[2]. Further complications are added by the development of an air core and the treatment of particle laden flows.

Modelling of the hydrodynamics within a hydrocyclone is a method by which to gain understanding of its flow features. The majority of models applied to the hydrocyclone are empirical in nature and relate a classification parameter (for example the cut size) with the dimensions and slurry properties[3]. However, a shortcoming of empirical models limits their application—the models can be used only in the experimental range of operating conditions and hydrocyclone geometries for which they were derived. This deficiency has necessitated the development of models through computational methods such as computational fluid dynamics (CFD).

This paper reports on preliminary work in the CFD modelling of two phase flow in a hydrocyclone, with the additional purpose to investigate the variation of device dimensions.

* Department of Process Engineering, University of Stellenbosch.
† Corresponding author.

Computational fluid dynamic modelling of two phase flow in a hydrocyclone

Table I

Proposed hydrocyclone dimensions

Hydrocyclone no.	1 Base case	2 Increase spigot	3 Decreased vortex finder
Hydrocyclone diameter (mm)	75	75	75
Inlet diameter (mm)	25	25	25
Vortex finder diameter (mm)	25	25	22
Spigot diameter (mm)	12.5	15	12.5
Vortex finder length (mm)	50	50	50
Cylindrical section length (mm)	75	75	75
Included cone angle (°)	20	20	20

The phases that were considered are water and air. Three geometries, based on the case study of Monredon *et al.*[4], were specified and simulations were performed in the commercial CFD package, FLUENT 6.3.

CFD modelling

Geometry construction and grid generation

The selected hydrocyclone dimensions are based on hydrocyclones no. 1, 2 and 3 of the Monredon case study[4]. The dimensions of these geometries are provided in Table I. Hydrocyclone no. 1 served as the base case geometry, while hydrocyclones 2 and 3 represented the variations of increased spigot diameter and smaller vortex finder respectively. The geometries were constructed with aid of the pre-processing package GAMBIT.

The implemented grid design is an adaptation of the one used in the study performed by Slack *et al.*[5]. An unstructured hexahedral mesh was applied to the main body of the hydrocyclone, as this type of mesh is more tolerant of high aspect ratios. To further avoid the occurrence of numerical diffusion, these cells were aligned in the flow direction. Due to the complexity caused by the tangential inlet, a tetrahedral mesh was applied. This mesh type allowed easier adjustment to the region where the inlet joins up with the body of the hydrocyclone. As the grid nodes of the main body and inlet volumes did not line up, a non-conformal interface was also used. The interface allows the pregeneration of data at the inlet to be built in and linked to the model.

Grid sizes were determined by ensuring that each grid was sufficiently fine to achieve grid independence. As a result, the number of cells used for the hydrocyclone geometries ranged between 250 000 and 270 000. The mesh, generated for hydrocyclone no. 1 is illustrated in Figure 1.

Boundary conditions

The computational domain was defined to begin at the tangential inlet where the feed stream was injected. The boundary condition at the inlet was determined from the operating mass flow rate (as obtained from the experimental work performed by Monredon *et al.*[4]). For the water-only feed stream with a mass flow of 67 kg/min, the associated velocity of 2.28 m/s was specified as the boundary condition.
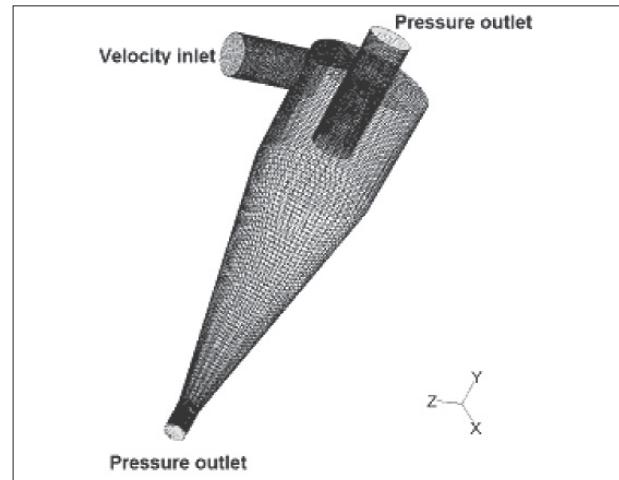

Figure 1—Hydrocyclone geometry illustrating mesh structure and assignment of boundary conditions

The outlet bounds of the system were defined as both the spigot and overflow discharge and pressure outlet boundary conditions of standard atmospheric pressure was applied. No-slip boundary conditions were also used for the wall of the hydrocyclone. At the point at which air core inception was desired, the backflow volume fraction of air at both discharge orifices were set to 1. The assignment of boundary conditions is illustrated in Figure 1.

Mathematical models

Turbulence modelling

FLUENT employs the Reynolds-averaging method to avoid the direct simulation of small-scale turbulent simulations. By means of this method, the continuity of mass and momentum are expressed by Equations [1] and [2] respectively.

$$\frac{\partial \rho}{\partial t} + \frac{\partial}{\partial x_i}(\rho u_i) = 0 \qquad [1]$$

$$\frac{\partial}{\partial t}(\rho u_i) + \frac{\partial}{\partial x_j}(\rho u_i u_j) = -\frac{\partial p}{\partial x_i} + \frac{\partial}{\partial x_j}\left[\mu\left(\frac{\partial u_i}{\partial x_j} + \frac{\partial u_j}{\partial x_i} - \frac{2}{3}\delta ij\frac{\partial u_l}{\partial x_l}\right)\right] + \frac{\partial}{\partial x_j}(-\rho\overline{u_i' u_j'}) \qquad [2]$$

where u_i denotes the velocity component.

Closure for the unknowns in the above equations can be obtained by the application of suitable turbulence models. The choice of the appropriate turbulence model is critical and should be made based on the complexity of flow physics, the required accuracy, the time period available for simulations and accessible computational resources[6].

For the modelling of the highly swirling flow of a hydrocyclone, the Reynolds stress model (RSM) is deemed to be an appropriate choice. Compared to the Boussinesq approach (employed in Spalart-Allmaras, k-ε and k-ω models), the RSM takes the true behaviour of the turbulent viscosity into consideration and therefore provides better approximations.

Computational fluid dynamic modelling of two phase flow in a hydrocyclone

The RSM is used to calculate the Reynolds stresses from differential transport equations, as represented by Equation [3].

$$\frac{\partial}{\partial t}\left(\rho\overline{u_i'u_j'}\right)+\frac{\partial}{\partial x_k}\left(\rho u_k\overline{u_i'u_j'}\right)=$$

$$P_{ij}+F_{ij}+G_{ij}+D_{ij}^T+D_{ij}^L+\Phi_{ij}-\varepsilon_{ij}$$

[3]

The second term on the left-hand side, $\frac{\partial}{\partial x_k}\left(\rho u_k\overline{u_i'u_j'}\right)$, is commonly referred to as the convection term, C_{ij}. P_{ij}, accounts for the stress production, while F_{ij} and G_{ij} represent the system rotation and buoyancy production. Turbulent and molecular diffusion are denoted by D_{ij}^T and D_{ij}^L respectively. The remaining terms, Φ_{ij} and ε_{ij}., symbolize pressure strain and dissipation.

Multiphase modelling

The selection of the volume of fluid (VOF) model as multiphase model was largely based on the fact that the water-air interaction in a hydrocyclone can be described as free surface flow. Studies such as that of Narashima *et al.*[7], further advocate the applicability of the VOF in the modelling of multiphase interactions of a hydrocyclone. To track the interface between the phases, the continuity equation is solved for the volume fraction of each phase:

$$\frac{1}{\rho_q}\left[\frac{\partial}{\partial t}\left(\alpha_q\rho_q\right)+\nabla\cdot\left(\alpha_q\rho_q\overrightarrow{v_q}\right)=\right.$$

$$\left.S_{\alpha q}+\sum_{p=1}^{n}\left(\dot{m}_{pq}-\dot{m}_{qp}\right)\right]$$

[4]

The volume fraction of phase q is represented by α_q. $\dot{m}_{pq}$ is the mass transfer from phase q to p and $S_{\alpha q}$ represents a source term.

Solver execution

To initialize an unsteady state analysis, pressure and velocity fields were pre-established through simulation of a water only phase field. On activation of transient conditions, air core inception was brought about by setting the air backflow volume fractions to unity. As the pressure field was pre-established, there was no need for patching of air in the system. To ensure that flow features were fully developed, transient simulations were allowed to run for at least one total flow time (mean residence time).

The convergence criteria of the unsteady analysis were set to 1×10^{-5}. To improve convergence the second order upwind and QUICK schemes were used and activated sequentially in the order as presented. The use of the VOF model necessitated the application of the segregated solver. PRESTO! was used as the pressure interpolation scheme, and SIMPLE proved to be adequate for pressure-velocity coupling.

Results

The results in this section present general trends in pressure and velocity field distributions that pertain to all three hydrocyclone geometries. As part of the investigation into the pressure field distribution, the multiphase interactions are researched by studying the air core development. Regarding the velocity field predictions, the three velocity components of hydrocyclone flow were considered: tangential, axial and radial velocity. The effect of varying device dimensions is highlighted where dissimilarities in results occurred.

Pressure field predictions and air core development

For initial conditions, where a water-only phase field was simulated, a negative core region was established. On initiation of air backflow under multiphase conditions, the air core evolved as illustrated in Figure 2: inception takes place at both the underflow and overflow orifices. The air core then extends throughout the body of the hydrocyclone along the pre-established sub-atmospheric core region. Air core development is completed as the two sections meet.

Attempts were made to initialize air core formation without the pre-establishment of a sub-atmospheric zone. In such cases, however, extremely divergent behaviour was exhibited. This dependency of air core formation on pre-established pressure fields supports the common understanding that air core formation is pressure driven.

Through the investigation of a variation in device dimensions it was further found that the air core diameter increases with an increase in the spigot diameter. Scaled plots
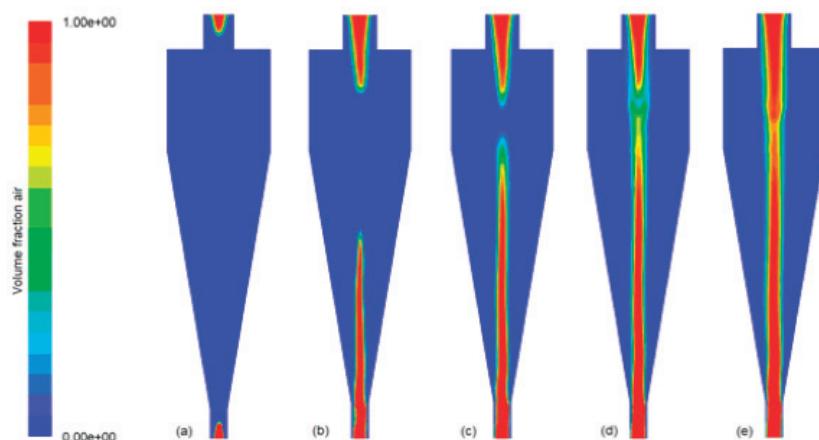

Figure 2—Development of air core at (a) 0.023 s (b) 0.068 s (c) 0.093 s (d) 0.126 s (e) 0.776 s

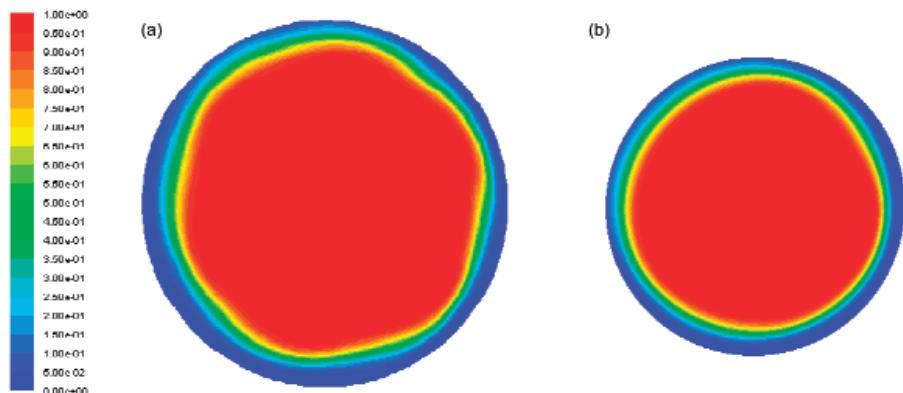# Computational fluid dynamic modelling of two phase flow in a hydrocyclone

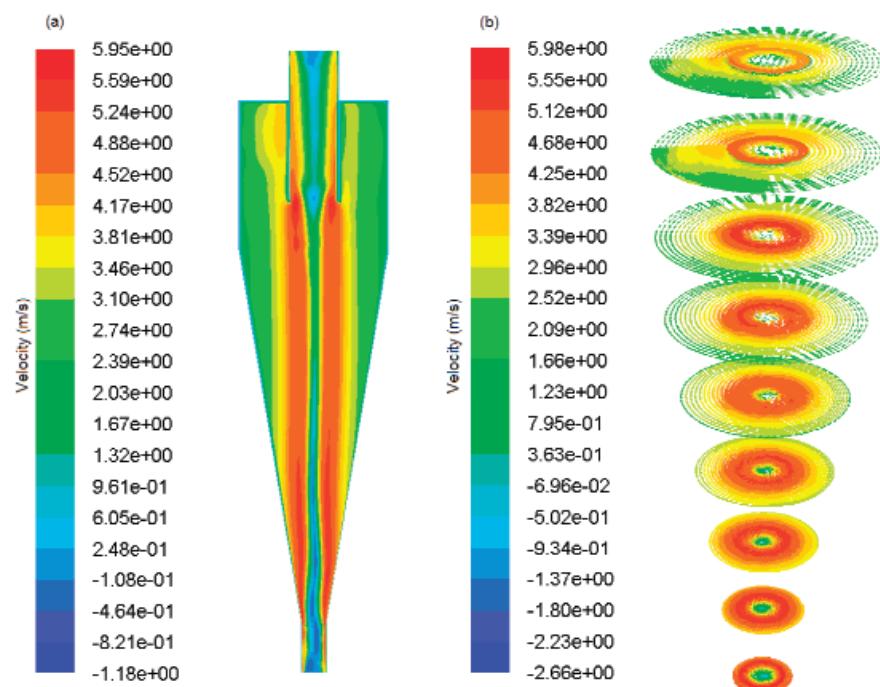Figure 3—Planar view of underflow outlet for (a) hydrocyclone no. 2 and (b) hydrocyclone no.3

Figure 4—Tangential velocity distribution of water and air system: (a) contour plot (b) vector plane plots

of the spigot surface for hydrocyclones no. 2 and 3 are used to illustrate this behaviour (refer to Figure 3). From the plot it is seen that the air core almost completely fills the cross-sectional area of the spigot, except for the band through which water is discharged. The increase in the cross-sectional area therefore results in an increase of the air core diameter.

Velocity field prediction

Tangential velocity

The tangential velocity field distribution of the multiphase system is illustrated in Figure 4 (a) and (b). Maximum positive values are noted in the regions peripheral to the central axis while very small regions of stagnant and reversed flow extend from both the spigot and vortex finder. As example, predicted liquid tangential velocity profiles, at horizontal intersections of 60 mm and 120 mm, are depicted in Figure 5 (a) and (b). A significant increase in the

tangential velocity occurs traversing from the wall inwards. At a point interfacing with the air core, the tangential velocity starts to decrease. This behaviour is indicative of the prominent flow feature, the Rankine vortex. By qualitative comparison, the predicted trends were also found to be consistent with experimental measurements of Monredon et al.[4].

The influence of different device dimensions on the tangential velocities is illustrated in Figure 5 (a) and (b). By comparing results from hydrocyclones no. 1 and 2, it is seen that the shape and magnitude of the tangential velocity stay relatively unchanged if the spigot diameter is increased. As with the Monredon et al. study[4], an increase in the tangential velocity is observed with a decrease in the vortex finder diameter. The velocity profile at 120 mm suggests that the influence of a decreased vortex finder becomes smaller with an increase in vertical depth.
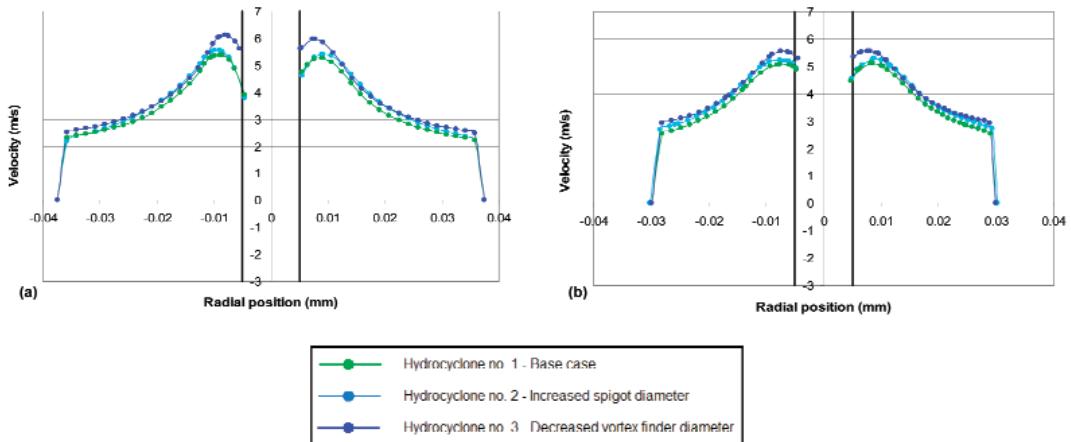
Figure 5—Predicted tangential velocity profiles at (a) 60 mm depth and (b) 120 mm depth
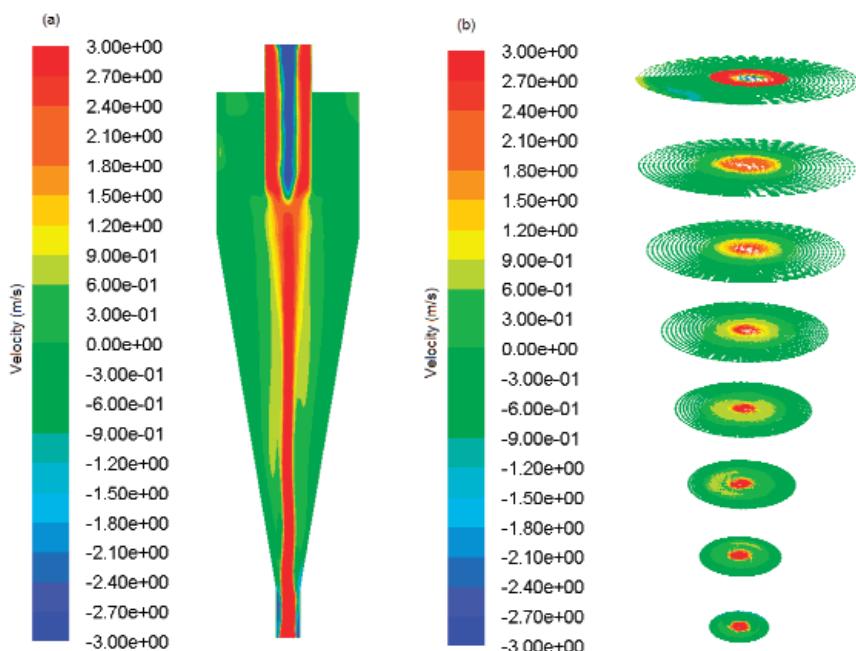

Figure 6—Axial velocity distribution of water and air system: (a) contour plot (b) vector plane plots

Axial velocity

The contour and vector plane plots of Figure 6 (a) and (b) provide the axial velocity distributions obtained for the water and air system. By inspection it is revealed that axial flow reversal is predicted—a positive core region (red and yellow) is contrasted with a negative or downward flow region (dark shade of green). This flow reversal signifies the presence of the locus of zero vertical velocity (LZVV). The LZVV is commonly associated with the distribution between the underflow and overflow stream. Particles on the outside of the LZVV will be rejected as underflow, while particles on the inside will be taken up in the overflow stream. The existence of the LZVV is manifested on the predicted velocity profiles as a point of zero velocity (refer to Figure 7 (a) and (b)). From these profiles it is further seen that the axial velocity increases in both the upward and downward direction from the LZVV. On a qualitative basis, the shape of the predicted

axial velocity profiles displayed excellent correlation with experimental measurements of Monredon et al.[4]. Concerning the variation in device dimensions, it is noted that the axial velocity profiles obtained for all three hydrocyclones are similar.

Radial velocity

Simulation results show irregular positive and negative radial velocity fields. Due to complexities involved with the measurement of the radial velocity, very little information is available about this velocity component. In practice, the tangential and axial velocities are usually measured, while the radial component is determined from the continuity equation. The irregularly distributed radial velocity fields, however, correspond with recent reports by Dlamini[8] and Cullivan et al.[9]. The velocity profiles further indicate that the magnitude of the radial component is much smaller than that

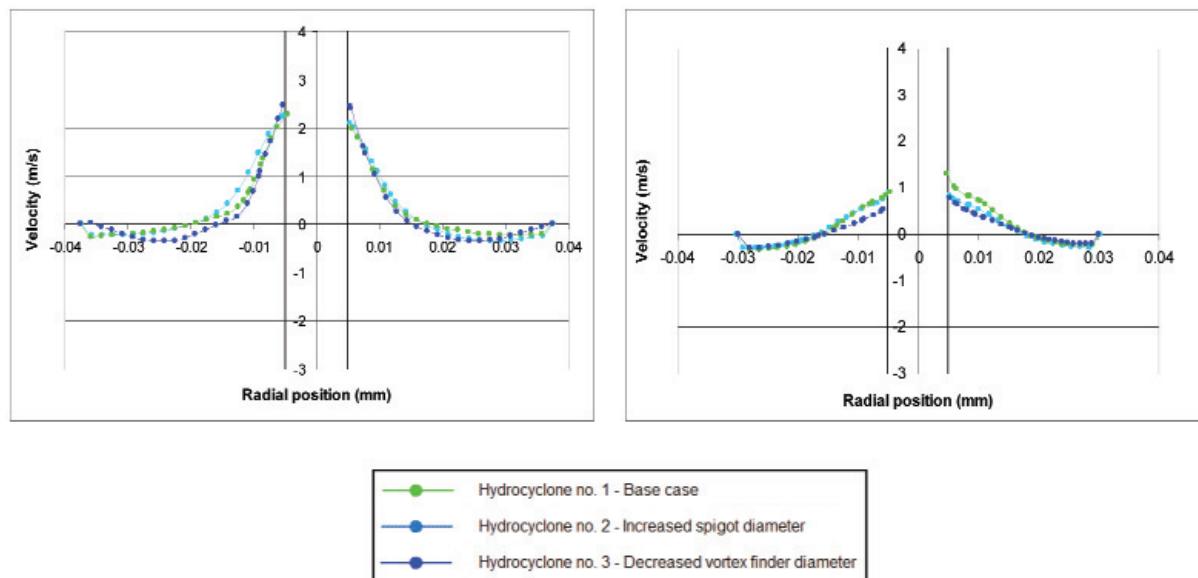# Computational fluid dynamic modelling of two phase flow in a hydrocyclone

Figure 7—Predicted axial velocity profiles at (a) 60 mm depth and (b) 120 mm depth

of the tangential or axial component. This characteristic agrees with work by Kelsall[10]. The variation in device dimensions does not seem to influence the radial velocity distributions as the predicted profiles for the three different hydrocyclone geometries indicated very little dissimilarities.

Split flow ratio

The effect of varying device dimensions was also noticed in the split flow ratios. For the base case geometry, hydrocyclone no. 1,7% of the feed stream reports to the underflow, while the corresponding value for hydrocyclone no. 2 is 14%. The increase in the underflow stream with an increase in spigot diameter is consistent with results by Monredon et al.[4]. This behaviour might be attributed to the fact that more water is allowed to escape through the underflow and less flow reversal is experienced.

Conclusions

Considering the fact that the main objective of this study was to set up a preliminary model of flow in a hydrocyclone, CFD modelling proved to be a valuable tool in providing an understanding of its complex three-dimensional flow and multiphase interactions. To obtain true representations of the internal flow, a transient simulation employing the RSM and VOF was implemented. From the resultant multiphase interaction, it is deduced that the sub-atmospheric core is a significant feature of the pressure field distribution and that air core formation is dependent on its pre-establishment. Concerning velocity field distributions, it is evident that CFD modelling is useful in providing accurate predictions of general flow trends and important features such as the Rankine vortex and LZVV. Ultimately, the application of CFD as a design tool is supported by the fact that it is effective in predicting the effect of varying device dimensions and yields results, which are consistent with experimentally measured work.

References

1 NARASIMHA, M., SRIPRIYA, R., and BANERJEE, P.K. CFD modelling of hydrocyclone—prediction of cut size, *International Journal of Mineral Processing*, vol. 75, 2005, p. 53–68.

2 DYAKOWSKI, T. and WILLIAMS, R.A. Modelling turbulence flow within a small diameter hydrocyclone, *Chemical Engineering Science*, vol. 48, 1993, p. 211–244.

3 DLAMINI, M.F., POWELL, M.S., and MEYER, C.J. A CFD simulation of a single phase hydrocyclone flow field, *The Journal of The South African Institute of Mining and Metallurgy*, vol. 105, 2005, p. 711–717.

4 MONREDON, T.C., HSIEH, K.T., and RAJAMANI, R.K. Fluid flow model of the hydrocyclone: an investigation of device dimensions, *International Journal of Mineral Processing*, vol. 35, 1992, p. 65–83.

5 SLACK, M., DEL PORTE, S., and ENGELMAN, M.S. Designing automated computational fluid dynamics tools for hydrocyclone design, *Minerals Engineering*, vol. 17, 2004. p. 705–711.

6 FLUENT, FLUENT 6.3 User Manual, Available at: http://www.fluent.com, Date accessed: 8 May 2007.

7 NARASIMHA, M., BRENNAN, M., and HOLTHAM, P.N. Large eddy simulation of hydrocyclone—prediction of air-core diameter and shape, *International Journal of Mineral Processing*, vol. 80, 2006, p. 1-14.

8 DLAMINI, M.F. Application of CFD to hydrocyclone flow prediction, Master Thesis, University of Cape Town, South Africa, 2004.

9 CULLIVAN, J.C., WILLIAMS, R.A., and CROSS, C.R. Understanding the hydrocyclone separator through computational fluid dynamics, *Transactions Institute Chemical Engineering Science*, vol. 81, 2003, p. 455–466.

10 KELSALL, D.F. A study of the motion of solid particles in a hydraulic cyclone, *Transactions Institute Chemical Engineering Science*, vol. 30, 1952. p. 87–104. ◆